nature structural & molecular biology

THAP proteins target specific DNA sites through bipartite recognition of adjacent major and minor grooves

Alex Sabogal[1,4], Artem Y Lyubimov[1,2,4], Jacob E Corn[1], James M Berger[1,2] & Donald C Rio[1–3]

THAP-family C_2CH zinc-coordinating DNA-binding proteins function in diverse eukaryotic cellular processes, such as transposition, transcriptional repression, stem-cell pluripotency, angiogenesis and neurological function. To determine the molecular basis for sequence-specific DNA recognition by THAP proteins, we solved the crystal structure of the *Drosophila melanogaster* P element transposase THAP domain (DmTHAP) in complex with a natural 10-base-pair site. In contrast to C_2H_2 zinc fingers, DmTHAP docks a conserved β-sheet into the major groove and a basic C-terminal loop into the adjacent minor groove. We confirmed specific protein-DNA interactions by mutagenesis and DNA-binding assays. Sequence analysis of natural and *in vitro*–selected binding sites suggests that several THAPs (DmTHAP and human THAP1 and THAP9) recognize a bipartite TXXGGGX(A/T) consensus motif; homology suggests THAP proteins bind DNA through a bipartite interaction. These findings reveal the conserved mechanisms by which THAP-family proteins engage specific chromosomal target elements.

Recent genome-sequencing efforts have identified the THAP domain, originally characterized as the N-terminal site-specific DNA-binding domain of the P element transposase of *D. melanogaster*[1,2], in over 300 proteins from animal genomes and parasitic mobile elements[3–6]. Approximately 80 residues long, THAP domains are characterized by a Cys-$X_{2–4}$-Cys-$X_{35–50}$-Cys-X_2-His zinc-coordinating motif and other signature elements, including a C-terminal AVPTIF sequence[4,7]. Mutations of these conserved sequence elements disrupt folding and DNA binding *in vitro*[1,8,9], and genetic studies have implicated mutated or truncated versions of these sequences in human neurological diseases[9]. THAP domains are the second most common zinc-coordinating DNA-binding domain after the C_2H_2 class of zinc fingers[4,10,11]. As is typical of large DNA-binding protein families, primary sequence conservation among THAP homologs is low[11], although secondary and tertiary structures, particularly the characteristic βαβ fold, are strongly conserved[7,12].

The phylogenetic distribution of THAP proteins (which includes evidence of a recently active P element transposase–related THAP9 gene in zebrafish[13]), combined with the absence of THAPs in non-animal species, suggests that the domain was recently incorporated into eukaryotic genomes by domestication of an ancestral mobile element[5,13]. More generally, THAP proteins are thought to share a common ancestral DNA-binding fold with the P element transposase[4,5]. Other features often shared between the THAP family of transcription factors and P element transposases include: (i) the stereotypical location of the THAP domains at the N termini of their resident open reading frames; (ii) a basic nuclear localization signal (NLS; residues 64–67 in DmTHAP) embedded within or near the THAP domain; and (iii) a C-terminal leucine-zipper or coiled-coil dimerization domain (residues 100–150 in P element transposase). These features allow THAP-family transcription factors to enter the nucleus, bind to DNA with high affinity and form higher-order oligomeric complexes with regulatory components, thereby linking DNA-targeting functions with the regulation of chromatin remodeling and transcriptional repression[14,15]. Signature THAP sequence elements, including the C_2CH zinc-coordinating motif, are found in 12 human proteins, several of which have been functionally characterized as nuclear DNA-binding proteins (THAP0 (ref. 16), THAP1 (ref. 17), THAP5 (ref. 18), THAP7 (ref. 14) and THAP11 (ref. 19)). At present, the mechanism by which THAP proteins recognize specific DNA sequences is unknown. Molecular insights into recognition are key to understanding how THAP-family transcription factors are targeted to chromosomal sites to modulate cellular processes. Indeed, many of the cellular THAP proteins studied to date act as transcription factors that control the expression of diverse sets of genes implicated in angiogenesis, apoptosis, cell cycle regulation, stem cell pluripotency and epigenetic gene silencing[8,14,15,17,19,20]. THAP family members also have been implicated in a variety of human disease pathways, from angiogenesis[20] and heart disease[18] to neurological defects[9] and multiple types of cancer[20–22].

To better understand THAP-DNA interactions, we purified a minimal 77-residue THAP domain (DmTHAP) from the *D. melanogaster* P element transposase, which is necessary and sufficient for high-affinity DNA binding[1,2,7], and determined its crystal structure in complex with a naturally occurring 10-base-pair (bp) DNA site. Our results show that DmTHAP specifically recognizes sequence elements in a bipartite manner using both the major and minor grooves of its target DNA site. Minor-groove recognition is achieved by a combination of

[1]Department of Molecular and Cell Biology, [2]California Institute for Quantitative Biosciences and [3]Center for Integrative Genomics, University of California, Berkeley, Berkeley, California, USA. [4]These authors contributed equally to this work. Correspondence should be addressed to D.C.R. (don_rio@berkeley.edu) and J.M.B. (jmberger@berkeley.edu).

Received 3 October; accepted 23 November; published online 13 December 2009; doi:10.1038/nsmb.1742

Table 1 Data collection and refinement statistics

	DmTHAP + 10 bp dsDNA
Data collection	
Space group	$P2_1$
Cell dimensions	
a, *b*, *c* (Å)	28.7, 69.3, 35.1
α, β, γ (°)	90.0, 92.5, 90.0
Wavelength (Å)	0.92
Resolution (Å)	50.0–1.74 (1.81–1.74)[a]
R_{sym}	0.049 (0.29)
$I/\sigma I$	21.6 (2.6)
Completeness (%)	95.0 (66.8)
Redundancy	3.5 (2.3)
Refinement	
Resolution (Å)	35.1–1.74
No. unique reflections	26,095 (1,841)
R_{work}/R_{free}	17.7/21.5
No. atoms	
Protein/DNA	1,001
Ligand/ion	1
Water	107
B-factors	
Protein/DNA	30.2
Ligand/ion	25.1
Water	36.6
R.m.s. deviations	
Bond lengths (Å)	0.011
Bond angles (°)	1.03

All data were collected from a single crystal.
[a]Values in parentheses are for highest-resolution shell.

direct base contacts and indirect sequence readout of DNA deformation through a variable, basic loop. By contrast, the adjacent major groove is sequence-specifically recognized by the central β-sheet of the domain. Due to their common ancestry, the sequence-specific DNA binding events of other THAP proteins can be postulated at a molecular level. In particular, the binding sites of two human THAPs (hTHAP1 and hTHAP9) seem to share common features with loci recognized by DmTHAP, including the sequence identity and spacing to create a TXXGGGX(A/T) consensus target motif. Contrary to proposed helix-groove models for THAP-DNA interactions[7], THAP domains instead engage appropriate target sites in complex genomes by a conserved bipartite β-sheet and loop-dependent readout mechanism.

RESULTS

Overall fold and secondary structure elements

To visualize how THAP proteins interact with specific DNA sequences, we determined the crystal structure of DmTHAP in complex with a naturally occurring 10-bp DNA site at 1.74-Å resolution by single-wavelength anomalous dispersion (SAD) methods. The quality of the resultant electron density maps (**Table 1**) allowed unambiguous mapping of both direct and water-mediated DNA-protein contacts. The final model includes the entire 10-bp DNA substrate and residues 1–76 of the transposase, excluding two disordered residues in loop 4 (Pro57 and Ala58) (**Fig. 1a**,**b**).

As expected, DmTHAP adopts a βαβ fold characteristic of THAP domains seen previously in apo NMR structures of human THAP1 and THAP2 and in the *Caenorhabditis elegans* C-terminal binding protein (CtBP)[7,12]. Structurally, the core fold of DmTHAP aligns well with those of other members of the THAP family (1.39, 0.71 and 1.46 Å r.m.s. deviation for hTHAP1, hTHAP2 and *C. elegans* CtBP, respectively; **Fig. 1c** and **Supplementary Fig. 1**). The rest of the molecule is composed of loops, of which loop 4 is the most variable in length, sequence and structure (**Fig. 1d** and **Supplementary Fig. 1**). DmTHAP binds DNA as a monomer, making a total of 17 direct and water-mediated base-specific contacts with two nonoverlapping regions that span the entire binding site (**Fig. 1e**). This interaction buries ~2,380 Å^2 of total surface area at the nucleoprotein interface.

Major-groove protein-DNA interactions

The main chain atoms of the N-terminal methionine (Met1) recognize the 3′ GA sequence from the major groove at positions 9 and 10 (**Figs. 1e**,**f** and **2a**). The β-sheet further interacts with the central GTGG sequence of the major groove, corresponding to positions 6–9 (**Figs. 1e**,**f** and **2b**). His18 and Gln42 from the two β-strands, along with the N terminus, make a total of six direct contacts with six bases and engage both strands of the DNA duplex in the major groove (**Figs. 1e**,**f** and **2b**). The main chain atoms of Tyr3, Leu16 and Asn40, along with the side chain of Gln42, further interact with five additional bases in the major groove via bridging water molecules (**Fig. 1e**). Given the variability of the residue composition in the THAP-domain β-sheet (**Fig. 1d**, **Supplementary Fig. 2**) and the ability of water to accommodate different hydrogen-bond donors and acceptors[23], the structure indicates that some THAP paralogs will be able to accommodate major-groove sequences that differ from that of DmTHAP.

Minor-groove protein-DNA interactions

Loop 4 (Arg65 and Arg67) interacts with the AT-rich sequence in the minor groove (positions 2–4, **Figs. 1e**,**f** and **2c**,**d**). Loop 4 is the most variable portion of THAP domains[4], yet at least one basic residue is found in this region (**Fig. 1d** and **Supplementary Figs. 1** and **3**). In DmTHAP, Arg65 contacts T7 directly and A4 through a bridging water molecule, while Arg67 makes water-mediated contacts with T3, A18 and A19 (**Figs. 1e** and **2c**,**d**). By contrast, Arg66 projects away from the DNA and occupies two conformations, both of which are engaged in π-stacking interactions with Trp53 (**Fig. 2e**). This residue structurally restricts one end of loop 4, directing the main chain to allow Arg65 and Arg67 to project into the minor groove. Arg66 also interacts with Asp45, Cys44 and His47, thus anchoring loop 4 to the zinc-coordinating core of DmTHAP. Together, the base of loop 4 and the central β-sheet create two ridges that project into adjacent DNA minor and major grooves, respectively (**Fig. 1f**).

In addition to direct contacts with bases in both grooves, indirect readout of deformable DNA sequences aids in specific site recognition by DmTHAP. The main chain atoms of Lys64, Arg65 and Arg66 all interact with the backbone phosphates of A19 and G6, resulting in a noticeable narrowing of the minor groove, which is localized to the region contacted by loop 4 (**Supplementary Figs. 4** and **5**). Distortions of local base pair geometry appear to be most pronounced at positions 2, 3 and 4, corresponding to minor groove binding by Arg65 and Arg67, as analyzed using the programs 3DNA and CURVES+ (**Supplementary Figs. 4** and **5**). However, it is unknown at this time if the DNA distortion is a result of DNA binding or is intrinsic to the DmTHAP binding sequence.

Validation of specific protein-DNA interactions by EMSA

We used electrophoretic mobility shift assays (EMSA) to determine the contributions of key residues in each groove toward the overall affinity (**Fig. 3a**,**b**). To examine the role of Met1, we deleted Tyr2 and Lys3, expecting that the truncated construct (ΔY2,K3) would perturb the position of the starting residue relative to the 3′ GA sequence. ΔY2,K3 had a partially reduced affinity by a factor of ~3 compared to wild-type DmTHAP (**Fig. 3a**,**c**), suggesting that the N terminus makes a modest contribution to the overall DNA-binding affinity. By contrast, the H18A

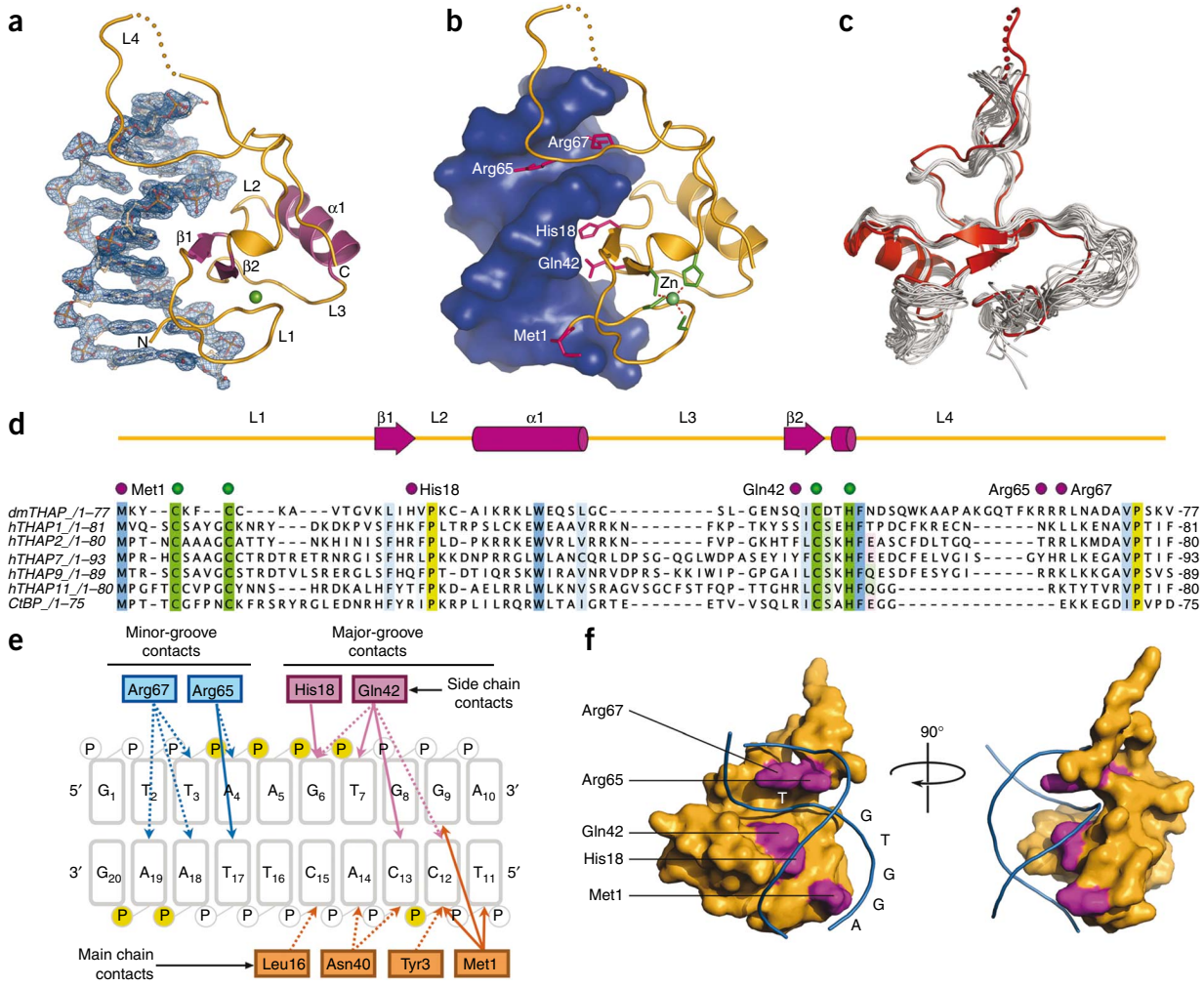

Figure 1 Structure of DmTHAP–DNA complex and specific interactions with DNA. (**a**) The protein-DNA interface. Experimental electron density map of the DNA (blue mesh) is contoured at 1.5σ. DmTHAP is shown as a ribbon diagram and labeled by secondary structure, with the βαβ motif highlighted in magenta. Zinc is shown as a green sphere. (**b**) Base-specific interactions in the major and minor grooves. Interacting residues are shown as magenta sticks; DNA is shown in blue surface representation; zinc-coordinating residues are shown as green sticks. (**c**) Structural alignment of DmTHAP (red) and the solution structure of human THAP2 (gray, PDB 2D8R). (**d**) Structure-based multiple sequence alignment of DmTHAP, human THAP1, THAP2, THAP7, THAP9 and THAP11 and *C. elegans* CtBP. Conserved residues are highlighted; zinc-coordinating C_2CH motif is highlighted in green and indicated by green circles; base-specific DNA-binding residues of DmTHAP are indicated by magenta circles and are labeled. The secondary structure diagram is shown for DmTHAP and labeled as in **a**. (**e**) Schematic representation of all base-specific contacts in the major and minor grooves. Direct contacts are shown as solid lines; base-specific water-mediated contacts are shown as dashed lines; interacting phosphates are highlighted yellow. (**f**) Surface representation of DmTHAP. Sequence-specific DNA-binding residues are highlighted in magenta. DNA backbone is shown as lines with subsite positions labeled.

and Q42A mutations substantially impaired DNA binding by a factor of ~12 and ~15 respectively, with the double H18A Q42A mutant protein showing an even greater reduction in affinity, by a factor of ~20 (**Fig. 3a**,**c**). The mutations R65A and R67A led to a similar loss of DNA binding by a factor of ~21 and ~17, respectively, with an even greater loss of binding for the R65A R67A double mutant by a factor of ~42 (**Fig. 3b**,**c**). The R66A mutation resulted in a complete loss of binding (**Fig. 3b**), which may be attributable to a possible destabilization of the core DmTHAP structure. Taken together, the biochemical analysis of base-specific contacts in both the major and minor grooves validates the DNA-protein interactions observed in the cocrystal structure.

Bipartite DNA targeting by other THAP proteins

Despite poor sequence conservation, the known tertiary structures of THAP proteins are highly similar, suggesting that the DNA recognition strategies used by DmTHAP are preserved among different THAP homologs. In support of this proposal, superposition of three previously reported DNA-free structures of hTHAP1, hTHAP2 and *C. elegans* CtBP[7,12] with the DNA-bound DmTHAP seen here results in plausible binding orientations for all proteins (**Supplementary Fig. 3**). In particular, each of these related THAP domains seems capable of interacting with DNA in a manner analogous to DmTHAP, with the conserved β-sheets of all three proteins docking into the major groove without steric hindrance (**Supplementary Fig. 3**). Homology-based structural models of all 12 human THAP proteins (hTHAP0–11) further indicate that the DNA-binding β-sheet is likely conserved across the THAP family (**Supplementary Fig. 2**). Although specific interactions with DNA cannot be inferred from these models, the apparent diversity of putative major groove–binding elements suggests that paralogous THAP domains likely recognize a variety of distinct target-site sequences

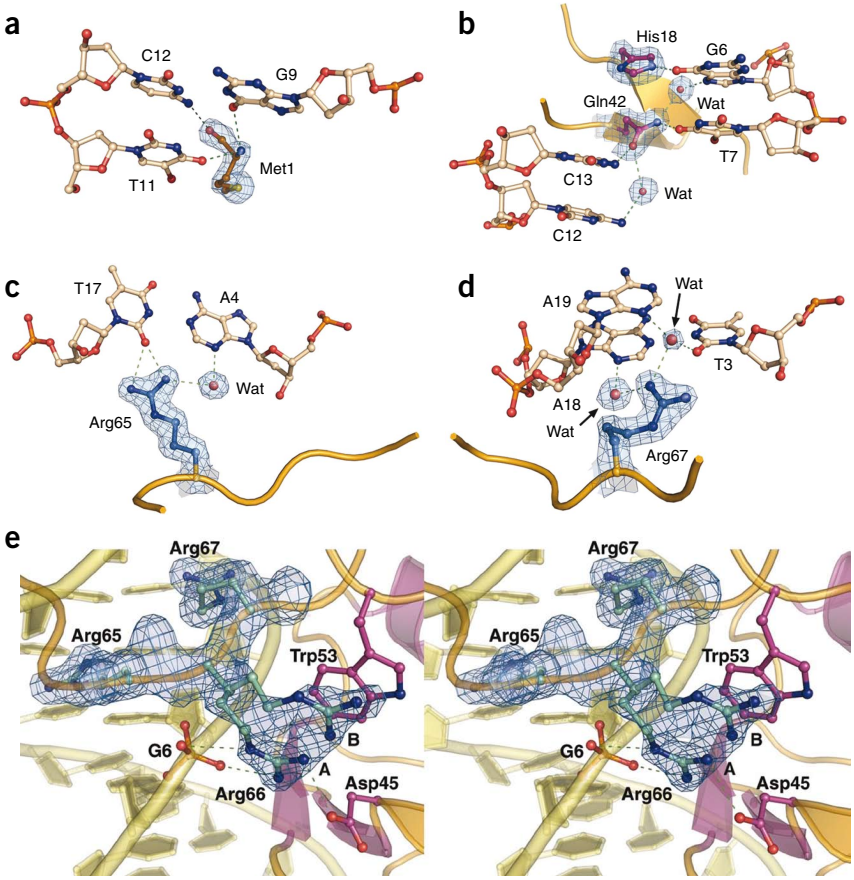

Figure 2 Base-specific DmTHAP–DNA contacts. (**a**–**d**) Interactions of Met1 (**a**), His18 and Gln42 (**b**), Arg65 (**c**) and Arg67 (**d**) with corresponding bases. Final electron densities (calculated using $2F_o - F_c$ coefficients and contoured at 1.5σ) are shown for interacting residues and bridging water molecules (Wat) only. A cartoon representation of the β-sheet is shown in **b**. (**e**) Stereographic representation of the RRR motif. Electron densities for Arg65, Arg67 and the alternate conformations of Arg66 are contoured at 1.0σ. Side chain atoms of the RRR motif, Trp53 and Asp45 as well as the phosphate atoms of G6 are shown in ball-and-stick representation.

in the major groove, most of which are unknown. Similarly, we note that the orientation of loop 4 with respect to the minor groove may also be variable, although in all cases some degree of engagement between this element and DNA can be modeled (**Supplementary Fig. 3**). Together, the structural models indicate that most THAP family members rely on a bipartite model for engaging DNA, and that the diversity of binding elements in the β-sheet likely correlates with a diversity of recognition sequences in the major groove.

THAP binding-site analysis

To determine whether THAP binding sites contain any signature sequence elements, we performed an alignment of experimentally verified natural target sites for DmTHAP[2,24] and hTHAP1 (ref. 20) with target sites determined by SELEX for human THAP1 (ref. 8) and THAP9. These alignments allowed us to divide known THAP-binding regions on the DNA into major and minor groove–interacting subsites (**Fig. 4**). The natural sites for the P element transposase and human THAP1, as well as the SELEX motifs for human THAP1 and THAP9, are all 9–11 bp in length. This metric seems to correspond to a single THAP domain binding site and is consistent with the ~10-bp DNA duplex used in our cocrystallization experiments.

Position 3 in the DmTHAP minor-groove subsite contains a conserved A-T base pair, which both interacts with the basic loop 4 and is a region of local distortion (**Figs. 1e**,**f** and **2d** and **Supplementary Figs. 4** and **5**). Notably, an A-T base pair is found at the same position in the hTHAP1 and hTHAP9 binding sites reported to date, suggesting that it is a critical recognition determinant for these proteins, as it is for DmTHAP (**Fig. 4**). Both hTHAP1 and hTHAP9 also contain at least one basic side chain in the loop 4 region (**Fig. 1d**), which could mediate binding the conserved A-T base pair in a manner analogous to DmTHAP. Moreover, in the SELEX motifs, the spacing between the conserved T at position 3 is ~5 bp, or 1 DNA half-turn, away from the next conserved sequence block (GGG or GGGCA), which comprises the major-groove subsite (**Fig. 4**); the spacing between the major- and minor-groove subsites is further restricted to 2 bp in all available THAP

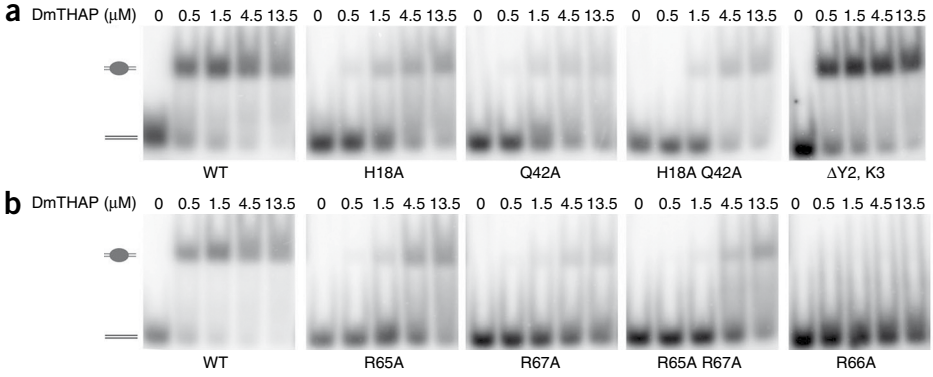

c

DmTHAP construct	K_D (μM)	K_D, mut / K_D, WT
WT	0.16	n/a
H18A	2.02	12
Q42A	2.48	15
H18A Q42A	3.24	20
R65A	3.36	21
R67A	2.82	17
R65A R67A	6.79	42
R66A	n/a	n/a
ΔY2,K3	0.47	3

Figure 3 Affinity determination of DmTHAP specificity mutants by EMSA. (**a**) Reduction in affinity observed in the major groove–binding mutants H18A, Q42A, H18A, Q42A and ΔY2,K3. (**b**) Reduction in affinity seen with the minor groove–binding mutants R65A, R67A, R65A, R67A and R66A. In each well, 1 nM of a radioactive 15-mer duplex DNA containing the specific transposase binding site was incubated with wild-type or mutant DmTHAP protein, allowed to equilibrate and then run on native 5% polyacrylamide gels. (**c**) Table of apparent K_d values and fold reduction compared to wild-type DmTHAP.

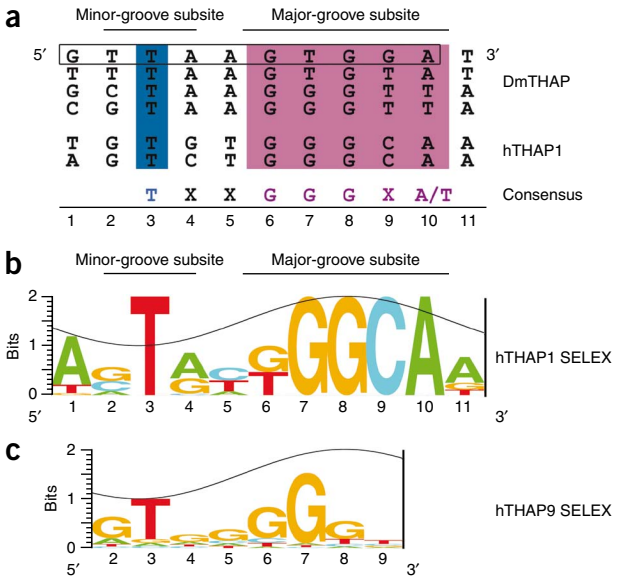

Figure 4 Bipartite sequence readout by THAP proteins. (**a**) Experimentally verified naturally occurring binding sites for the P element transposase and human THAP1. The consensus major and minor groove subsites are highlighted in magenta and blue, respectively. The sequence used for cocrystallization with DmTHAP is boxed. (**b**) Sequence logos made from position-specific scoring matrixes from SELEX experiments of human THAP1 (ref. 8) and (**c**) human THAP9. DNA helical phasing is represented as an 11-bp SIN wave and positioned based on DmTHAP structure.

target sites. The DmTHAP structure reveals that this spacing is necessary for the protein to arch over the DNA backbone and bind both grooves on the same face of the duplex (**Fig. 1f**). Taken together, these results suggest that a common core set of DNA sequence motifs may be conserved between DmTHAP and the THAP1 and THAP9 subfamilies.

DISCUSSION

DmTHAP uses a novel DNA-targeting mechanism

The ability of DmTHAP to use a β-sheet for recognizing the DNA major groove differs markedly from the binding mode employed by canonical C_2H_2 zif268 zinc fingers, to which it has been compared previously (**Fig. 5a**,**b**). The typical ~30-residue C_2H_2 zinc-finger motif presents an α-helix to the major groove of DNA[25]. Classical C_2H_2 zinc-finger proteins also are highly modular, recognizing extended DNA sequences through the use of several tandem copies of the domain[10,11,25]. By contrast, most THAP protein family members have only a single N-terminal THAP domain[4], possibly due to a need for the N-terminal amino group to contact DNA.

β-sheet–major groove interactions have been observed in other structures, such as the Arc and MetJ repressors[26], the N-terminal domain of the λ integrase[27] and the Tn916 transposase DNA-binding domain[28]. However, notable differences between these structures and DmTHAP also are present (**Fig. 5**). For example, the β-sheets of Arc and MetJ are composed of strands donated by individual subunits of a homodimer, whereas DmTHAP is monomeric. The λ integrase N-terminal domain is similar to DmTHAP in combining a major groove–binding β-sheet with a minor groove–binding element but uses a 3_{10} helix rather than a loop. The DNA-binding domain of Tn916 transposase uses a β-sheet to bind the major groove and a loop to engage the minor groove. However, the minor-groove contacts of the Tn916 DNA-binding domain are predominantly with the phosphate backbone rather than with the bases, and therefore they do not seem to be sequence specific. Overall, the RRR sequence of DmTHAP loop 4 is perhaps most reminiscent of the 'AT-hook' motif found in high-mobility group proteins[29], in which two arginine residues, separated by a single residue, insert into the minor groove to contact specific bases. Taken together, these comparisons indicate that THAP domains use a unique combination of DNA-recognition strategies to engage their target sites, allowing for the possibility of engineering novel DNA binding specificities.

Direct sequence readout by β-sheet side chains

The N terminus of THAP proteins, up to the first zinc-coordinating cysteine, is typically 2–4 residues long[4]. Therefore, it seems likely that an interaction between the N-terminal-most methionine and DNA is often preserved across the THAP family. By contrast, the β-sheet residues used by DmTHAP to bind DNA show remarkably little sequence conservation[4] (**Fig. 1d**). It seems likely that variation at these β-sheet positions, along with variation in the precise length and composition of the N terminus, alters the DNA sequence(s) recognized by the THAP proteins through the major groove. In agreement with this

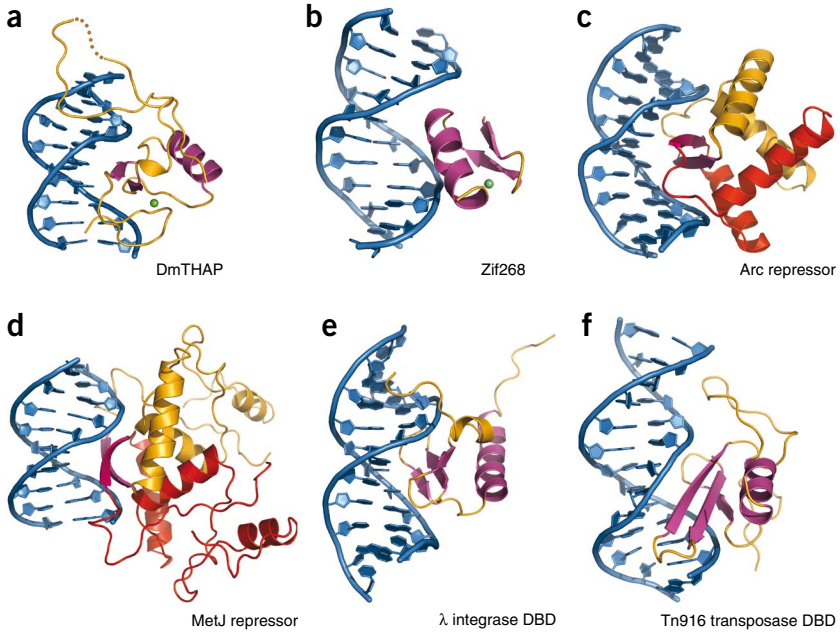

Figure 5 DmTHAP binds DNA in a manner distinct from the canonical zinc fingers. Cartoon representation of (**a**) DmTHAP and (**b**) Zif268 (PDB 1AAY (ref. 32)) in association with double-stranded DNA. Only a single Zif268 domain is shown. Also distinct from the THAP DNA-recognition interface are the homodimeric proteins (**c**) Arc repressor (PDB 1BDT (ref. 33)) and (**d**) MetJ repressor (PDB 1CMA (ref. 34)) each polypeptide colored in red and yellow. (**e**) λ-integrase (PDB 2WCC (ref. 27)) and (**f**) Tn916 integrase (PDB 1B69 (ref. 28)) DNA-binding domains may be the most similar to THAP domains. Secondary structure color schemes are the same as in **Figure 1a**.

premise, a previous study of a natural C-terminal deletion mutant repressor form of P element transposase assessed the effects of the H18A mutation by DNase I footprinting on its natural DNA-binding site[1] and found that, in the context of the truncated 207-residue KP repressor protein, the H18A mutant showed nonspecific DNA-binding behavior while retaining high affinity for DNA duplexes. Notably, the most highly conserved THAP domain residues seem to have structural roles in forming and stabilizing the hydrophobic core of the protein[7,12].

Loop 4 sequence affects DNA binding

Of all of the THAP proteins analyzed here, *C. elegans* CtBP has one of the shortest loop 4 regions. Although CtBP retains the consensus C-terminal AVPTIF motif, the internal truncation of loop 4 suggests that the protein may interact with the minor groove in a manner distinct from that of DmTHAP. Nonetheless, our modeling studies suggest that CtBP loop 4 does retain a pair of lysines that appear to be within interacting distance of the phosphate backbone or perhaps capable of projecting into the minor groove (**Fig. 1d** and **Supplementary Fig. 3d**). Human THAP11 (Ronin) has a loop 4 similar to CtBP and may bind DNA in an analogous fashion. By contrast, truncating the C terminus of DmTHAP at position 73 disrupts the AVPTIF motif (AVPSKV in DmTHAP), resulting in the destabilization of loop 4 and loss of DNA binding[1]. Thus, the molecular definition of a minimal THAP domain must include the AVPTIF motif to complete the fold and optimally position minor groove–binding residues.

A narrowing of the minor groove is observed at the positions bound by the basic loop 4 in DmTHAP, where it likely contributes to DNA site selection by indirect readout (**Supplementary Figs. 4** and **5**). This phenomenon may be present in other THAPs. For example, the SELEX-derived motifs of several monomeric THAP binding sites indicate that the information content in the minor-groove position 3 is higher than background (≥1) for both hTHAP1 and hTHAP9 (**Fig. 4**), consistent with high minor-groove conservation signatures and distorted DNA observed in several replication proteins[30].

Bipartite DNA-binding model applied to human THAP1

The bipartite binding model presented here can be used to explain several biochemical and biophysical observations of hTHAP1, as well as the molecular basis for generalized human dystonia (DYT6) in adults[9]. For example, EMSA studies of hTHAP1 using an *in vitro*–derived 11-bp target sequence (known as THABS, AGTAAGGGCAA) showed binding defects when the core TXXGGGCA recognition motif was mutated[8]. Our model suggests these defects are likely to be caused by the disruption of key major- and minor-groove interactions. In the same system, NMR experiments showed measurable changes in chemical shifts occurring upon DNA addition that could be associated with residues identified here as important for DNA binding[7]. Although not a direct indicator of DNA binding, these data revealed large chemical shifts for several residues located in loop 4, which is disordered in the absence of DNA[7], presumably because of the docking of loop 4 to the minor groove. These observations, coupled with the hTHAP1 SELEX analysis and structural modeling described above, are consistent with a bipartite targeting mechanism for hTHAP1.

The DmTHAP–DNA structure similarly can explain the defects in genetically identified hTHAP1 mutants that cause DYT6 (ref. 9), a disease that results in abnormal or repetitive movements of the limbs as well as speech defects[31]. In one reported deletion mutant, hTHAP1 loop 4 is truncated upstream of the AVPTIF motif that is needed to complete the THAP fold and help position basic residues to bind the minor-groove subsite. This deletion, as well as a single point mutant, F81L (affecting the phenylalanine position in the AVPTIF motif), has been shown to substantially reduce DNA binding[9]. Phe81 sits far from the DNA-binding interface but within the AVPTIF motif, and thus it may also affect DNA binding by destabilizing the structure of loop 4. Alternatively, the F81L substitution could affect other aspects of DNA binding in the context of dimeric full-length hTHAP1.

The downstream consequences of DNA-binding defects of hTHAP1 are believed to include a reduced repression of hTHAP1 target genes, resulting in aberrant transcriptional programs for genes involved in cell-cycle control and growth[17,20]. Thus, structural information from the DmTHAP–DNA complex can link substitution or deletion of specific residues to disruption of neurological function through the role of these residues in DNA binding and structural stability. Furthermore, putative hTHAP1 binding sites can now be better identified with the understanding of how they are recognized by THAP domains. Knowledge of the molecular mechanism of specific DNA site recognition by THAP domains should facilitate the further study of the downstream effects of DNA binding.

THAP domain oligomerization and regulation

Although single THAP domains bind to DNA as monomers, many family members are predicted to form dimers (or possibly higher-order oligomers) through a common C-terminal leucine-zipper–coiled-coil motif[2]. Dimerization allows for multisite DNA binding in THAP proteins, exemplified by the *D. melanogaster* P element transposase[2] and postulated for human THAP11 (Ronin), which has a 20-bp binding site and a predicted leucine-zipper domain[19,22]. Though uncommon, proteins containing multiple THAP domains do exist[4]; an extreme example is the open reading frame CG10631 from *D. melanogaster*, with 27 tandem THAP domains and no known function[4]. Furthermore, hTHAP7 and hTHAP11 are found together in a transcriptional repression complex[19], which may use several THAP domains for complex multisite and multisequence binding events. Regulation of DNA binding by THAP proteins also is postulated to occur for certain THAP homologs. For example, the THAP1 and THAP5 mRNAs are predicted to be alternatively spliced such that one isoform lacks a complete THAP domain, whereas the *D. melanogaster* transcriptional corepressor, CtBP, lacks the DNA-binding THAP element found in its *C. elegans* counterpart[6].

In summary, our structure provides the first general model for DNA recognition by the abundant THAP-domain protein family. THAP domains comprise a unique class of C_2CH zinc-coordinating DNA-binding folds which, in contrast to canonical C_2H_2 zinc fingers such as ZiF268, as well as the nuclear receptor superfamily and globin transcription factor 1 family[3,11], use a β-sheet to bind DNA in the major groove and make additional specific minor-groove protein-DNA contacts using a C-terminal basic loop. Based on structural, biochemical and bioinformatic results, we propose that THAP domains target DNA through a bipartite mechanism, with some family members targeting a consensus sequence of TXXGGGX(A/T) that bears readily identifiable major- and minor-groove subsites. Local variations in target DNA sequence can be accommodated by residue substitutions in the β-sheet and loop 4 as well as (to a lesser extent) changes to N-terminal length and sequence. The structural insights presented here significantly advance our knowledge of THAP-domain function and the mechanism of sequence-specific protein-DNA recognition. This analysis should aid in the understanding of yet-unstudied biological processes in humans and diverse animals that depend on THAP domain–containing DNA-binding proteins.

METHODS

Methods and any associated references are available in the online version of the paper at http://www.nature.com/nsmb/.

Accession codes. Protein Data Bank: coordinates and structure factors for the DmTHAP–DNA complex have been deposited with accession code 3KDE.

Note: Supplementary information is available on the Nature Structural & Molecular Biology website.

ACKNOWLEDGMENTS

The authors would like to thank J. Gureasko and J. Kuriyan (Univ. California, Berkeley) for use of equipment and technical expertise, E. Abbate and M. Botchan (Univ. California, Berkeley) for crystallography supplies and experimental design, N. Echols and T. Alber (Univ. California, Berkeley) for use of equipment and assistance with data collection, J. Holton for assistance with data collection, A. May (Fluidigm) for crystallography supplies and assistance with data collection, D. King (Univ. California, Berkeley, and Howard Hughes Medical Institute Mass Spectrometry Laboratory) for MS analysis, N. Ogowa and M. Biggin (Univ. California, Berkeley) for reagents and expertise for the SELEX protocol, R. Schultzaberger and M. Eisen for assistance with SELEX data analysis and for creating the sequence logos, K. Collins for data analysis and D. Wemmer, M. Levine and M. Botchan for critical reading of the manuscript. A.Y.L. is supported by an American Cancer Society postdoctoral fellowship, J.M.B. by the US National Cancer Institute (CA077307) and D.C.R. by the National Institute of General Medical Sciences (GM61987).

AUTHOR CONTRIBUTIONS

A.S. and D.C.R. conceived the experiments; D.C.R. synthesized brominated DNA oligonucleotides; A.S. purified the proteins and nucleic acids and crystallized the complex; J.E.C., A.Y.L. and J.M.B. provided guidance in crystallography trials; A.Y.L. and A.S. collected and analyzed the structural data; J.M.B. assisted with model building and refinement; A.Y.L. solved the structure and made all structural models; A.S. performed the DmTHAP mutagenesis and biochemistry, the SELEX experiment for human THAP9 and the THAP DNA-binding-site sequence analysis; A.S., A.Y.L., J.M.B. and D.C.R. wrote the paper.

Published online at http://www.nature.com/nsmb/.
Reprints and permissions information is available online at http://npg.nature.com/reprintsandpermissions/.

1. Lee, C.C., Beall, E.L. & Rio, D.C. DNA binding by the KP repressor protein inhibits P-element transposase activity in vitro. *EMBO J.* **17**, 4166–4174 (1998).
2. Lee, C.C., Mul, Y.M. & Rio, D.C. The *Drosophila* P-element KP repressor protein dimerizes and interacts with multiple sites on P-element DNA. *Mol. Cell. Biol.* **16**, 5616–5622 (1996).
3. Finn, R.D. *et al.* The Pfam protein families database. *Nucleic Acids Res.* **36**, D281–D288 (2008).
4. Roussigne, M. *et al.* The THAP domain: a novel protein motif with similarity to the DNA-binding domain of P element transposase. *Trends Biochem. Sci.* **28**, 66–69 (2003).
5. Quesneville, H., Nouaud, D. & Anxolabehere, D. Recurrent recruitment of the THAP DNA-binding domain and molecular domestication of the P-transposable element. *Mol. Biol. Evol.* **22**, 741–746 (2005).
6. Nicholas, H.R., Lowry, J.A., Wu, T. & Crossley, M. The *Caenorhabditis elegans* protein CTBP-1 defines a new group of THAP domain-containing CtBP corepressors. *J. Mol. Biol.* **375**, 1–11 (2008).
7. Bessiere, D. *et al.* Structure-function analysis of the THAP zinc finger of THAP1, a large C2CH DNA-binding module linked to Rb/E2F pathways. *J. Biol. Chem.* **283**, 4352–4363 (2008).
8. Clouaire, T. *et al.* The THAP domain of THAP1 is a large C2CH module with zinc-dependent sequence-specific DNA-binding activity. *Proc. Natl. Acad. Sci. USA* **102**, 6907–6912 (2005).
9. Fuchs, T. *et al.* Mutations in the THAP1 gene are responsible for DYT6 primary torsion dystonia. *Nat. Genet.* **41**, 286–288 (2009).
10. Wolfe, S.A., Nekludova, L. & Pabo,, C.O. DNA recognition by Cys2His2 zinc finger proteins. *Annu. Rev. Biophys. Biomol. Struct.* **29**, 183–212 (2000).
11. Luscombe, N.M., Austin, S.E., Berman, H.M. & Thornton, J.M. An overview of the structures of protein-DNA complexes. *Genome Biol.* **1** reviews001.1–001.10 (2000).
12. Liew, C.K., Crossley, M., Mackay, J.P. & Nicholas, H.R. Solution structure of the THAP domain from *Caenorhabditis elegans* C-terminal binding protein (CtBP). *J. Mol. Biol.* **366**, 382–390 (2007).
13. Hammer, S.E., Strehl, S. & Hagemann, S. Homologs of *Drosophila* P transposons were mobile in zebrafish but have been domesticated in a common ancestor of chicken and human. *Mol. Biol. Evol.* **22**, 833–844 (2005).
14. Macfarlan, T. *et al.* Human THAP7 is a chromatin-associated, histone tail-binding protein that represses transcription via recruitment of HDAC3 and nuclear hormone receptor corepressor. *J. Biol. Chem.* **280**, 7346–7358 (2005).
15. Macfarlan, T., Parker, J.B., Nagata, K. & Chakravarti, D. Thanatos-associated protein 7 associates with template activating factor-Iβ and inhibits histone acetylation to repress transcription. *Mol. Endocrinol.* **20**, 335–347 (2006).
16. Lin, Y., Khokhlatchev, A., Figeys, D. & Avruch, J. Death-associated protein 4 binds MST1 and augments MST1-induced apoptosis. *J. Biol. Chem.* **277**, 47991–48001 (2002).
17. Roussigne, M., Cayrol, C., Clouaire, T., Amalric, F. & Girard, J.P. THAP1 is a nuclear proapoptotic factor that links prostate-apoptosis-response-4 (Par-4) to PML nuclear bodies. *Oncogene* **22**, 2432–2442 (2003).
18. Balakrishnan, M.P. *et al.* THAP5 is a human cardiac-specific inhibitor of cell cycle that is cleaved by the proapoptotic Omi/HtrA2 protease during cell death. *Am. J. Physiol. Heart Circ. Physiol.* **297**, H643–H653 (2009).
19. Dejosez, M. *et al.* Ronin is essential for embryogenesis and the pluripotency of mouse embryonic stem cells. *Cell* **133**, 1162–1174 (2008).
20. Cayrol, C. *et al.* The THAP-zinc finger protein THAP1 regulates endothelial cell proliferation through modulation of pRB/E2F cell-cycle target genes. *Blood* **109**, 584–594 (2007).
21. De Souza Santos, E., De Bessa, S.A., Netto, M.M. & Nagai, M.A. Silencing of LRRC49 and THAP10 genes by bidirectional promoter hypermethylation is a frequent event in breast cancer. *Int. J. Oncol.* **33**, 25–31 (2008).
22. Zhu, C.Y. *et al.* Cell growth suppression by thanatos-associated protein 11(THAP11) is mediated by transcriptional downregulation of c-Myc. *Cell Death Differ.* **16**, 395–405 (2009).
23. Luscombe, N.M., Laskowski, R.A. & Thornton, J.M. Amino acid-base interactions: a three-dimensional analysis of protein-DNA interactions at an atomic level. *Nucleic Acids Res.* **29**, 2860–2874 (2001).
24. Kaufman, P.D., Doll, R.F. & Rio, D.C. *Drosophila* P element transposase recognizes internal P element DNA sequences. *Cell* **59**, 359–371 (1989).
25. Pavletich, N.P. & Pabo, C.O. Zinc finger-DNA recognition: crystal structure of a Zif268-DNA complex at 2.1 A. *Science* **252**, 809–817 (1991).
26. Suzuki, M. DNA recognition by a β-sheet. *Protein Eng.* **8**, 1–4 (1995).
27. Fadeev, E.A., Sam, M.D. & Clubb, R.T. NMR structure of the amino-terminal domain of the λ integrase protein in complex with DNA: immobilization of a flexible tail facilitates β-sheet recognition of the major groove. *J. Mol. Biol.* **388**, 682–690 (2009).
28. Wojciak, J.M., Connolly, K.M. & Clubb, R.T. NMR structure of the Tn916 integrase-DNA complex. *Nat. Struct. Biol.* **6**, 366–373 (1999).
29. Geierstanger, B.H., Volkman, B.F., Kremer, W. & Wemmer, D.E. Short peptide fragments derived from HMG-I/Y proteins bind specifically to the minor groove of DNA. *Biochemistry* **33**, 5347–5355 (1994).
30. Schneider, T.D. Strong minor groove base conservation in sequence logos implies DNA distortion or base flipping during replication and transcription initiation. *Nucleic Acids Res.* **29**, 4881–4891 (2001).
31. Muller, U. The monogenic primary dystonias. *Brain* **132**, 2005–2025 (2009).
32. Elrod-Erickson, M., Rould, M.A., Nekludova, L. & Pabo, C.O. Zif268 protein-DNA complex refined at 1.6 Å: a model system for understanding zinc finger-DNA interactions. *Structure* **4**, 1171–1180 (1996).
33. Schildbach, J.F., Karzai, A.W., Raumann, B.E. & Sauer, R.T. Origins of DNA-binding specificity: role of protein contacts with the DNA backbone. *Proc. Natl. Acad. Sci. USA* **96**, 811–817 (1999).
34. Somers, W.S. & Phillips, S.E. Crystal structure of the met repressor-operator complex at 2.8 Å resolution reveals DNA recognition by β-strands. *Nature* **359**, 387–393 (1992).

ONLINE METHODS

Protein purification. We amplified residues 1–77 of the *Drosophila* P element transposase using the primers 5′-GCATGAAATCATATGAAGTACTGCAAGT TCTGC-3′ and 5′-GCGTACTTACCATGGTTACACCTTGGAGGGCACGGC GTC-3′, then subcloned the product into pRSETA (Invitrogen), using growth and expression as described for PN88 (ref. 1). We sonicated frozen cell pellets with 10 ml lysis buffer (25 mM HEPES-KOH, pH 7.6, 1 M NaCl, 10% (v/v) glycerol, 1 mM PMSF, 0.5 mM tris(2-carboxyethyl)phosphine (TCEP), 0.5 μg ml^{-1} each of leupeptin, pepstatin, aprotinin, antipain and chymostatin) per gram of frozen bacterial paste. We removed nucleic acids from clarified lysates by addition of 30 ml of Q Sepharose Fast Flow resin (Pharmacia) at 4 °C for 1 h. We diluted the flow-through five-fold with buffer A (25 mM HEPES-KOH, pH 7.6, 10% (v/v) glycerol), then filtered and loaded the material onto a 30-ml SP Sepharose Fast Flow column (Pharmacia) pre-equilibrated with 80% (v/v) buffer A and 20% (v/v) buffer B (25 mM HEPES-KOH, pH 7.6, 1 M NaCl, 10% (v/v) glycerol). We added $ZnSO_4$ and TCEP to final concentrations of 10 μM and 0.5 mM, respectively, to elutions. Following dialysis against 10% (v/v) buffer B plus 10 μM $ZnSO_4$, we loaded the solution onto an 8-ml heparin-agarose column, and DmTHAP was eluted with a linear gradient of 10–55% (v/v) buffer B. Again, $ZnSO_4$ and TCEP were added. Using a 120-ml Superdex 75 gel-filtration column (GE Healthcare), DmTHAP eluted as a monomer at ~10 kDa, and we concentrated it to ~20 mg ml^{-1} and froze aliquots in liquid nitrogen in gel-filtration buffer (10 mM HEPES-KOH, pH 8.0, 50 mM NaCl and 0.5 mM TCEP).

We made proteins for EMSA assays by adding a C-terminal hexahistidine tag to the DmTHAP construct. We made point mutants by overlapping-primer PCR and expressed them as described above for DmTHAP. We purified proteins using a 1-ml HiTRAP FF column as described by the manufacturer (Pharmacia), then spiked $ZnSO_4$ and TCEP to final concentrations of 10 μM and 0.5 mM, respectively, and loaded the material onto a 24-ml Superdex 75 column (Pharmacia). We froze aliquots in gel-filtration buffer as described above. We cloned hTHAP9 residues 1–94 into pRSETA (Invitrogen), added a C-terminal hexahistidine tag and purified it similarly.

Preparation of oligonucleotides. We synthesized brominated DNA oligonucleotides on Applied Biosystems model 392 DNA synthesizer at 1 μmol scale, with an overnight manual elution using 1.5 ml NH_4OH at 22 °C. We purified the oligonucleotides using 19% (w/v) polyacrylamide and 8.3 M urea denaturing gels, visualized them by UV shadowing, and extracted gel slices in TE buffer (10 mM Tris-HCl, 1 mM EDTA, pH 8.0) at 37 °C, then desalted the buffer with two rounds of ethanol precipitation. We resuspended purified single-strand oligonucleotides in 10 mM HEPES-KOH, pH 8.0 and 50 mM NaCl and then heated equimolar amounts of each to 65 °C and slowly cooled them.

EMSA assays. We performed EMSA assays with the oligos 5′-GAGGTTAA GTGGATGT-3′ and 5′-TACATCCACTTAAC-3′, purified as described above. We 5′ end–labeled the 15-mer duplex with T4 polynucleotide kinase (USB), γ-[^{32}P]ATP (GE Healthcare) and a P-6 column (Bio-Rad). We measured apparent K_d using 1 nM DNA with increasing protein in a 20-μl reaction volume (10 mM HEPES-KOH, pH 8.0, 50 mM NaCl and 10% (v/v) glycerol), for 30 min at room temperature and loaded the reaction onto a native 5% (w/v) polyacrylamide gel. We ran the gel for 1 h at 150 V at 4 °C, in 0.5× TBE buffer (0.089 M Tris base, 0.089 M boric acid, 2 mM EDTA, pH 8.35), dried and visualized the results using the Typhoon Phosphoimager system and then performed binding analysis using Prism5 (GraphPad Software).

Cocrystallization of DmTHAP with DNA. We used vapor diffusion methods with a Mosquito crystallization system (TTP LabTech) with 200 nl dropsize to produce diffraction-quality crystals in 24% (w/v) polyethylene glycol (PEG), MW 8000 (Fluka), 5 mM NaCl, 0.05 M 3-(cyclohexylamino)-2-hydroxy-1-propanesulfonic acid sodium salt, pH 9.0 (Hampton Research), 10 mM TCEP at 25 °C in ~3–5 d. For cryoprotection, we incubated the drop with 26% (w/v) PEG, molecular weight 8,000, 25 mM NaCl, 0.05 M 3-(cyclohexylamino)-2-hydroxy-1-propanesulfonic acid sodium salt, pH 9.0, 10 mM TCEP and 20% (v/v) xylitol. We collected diffraction data at the Advanced Light Source beamline 8.3.1 from a single crystal at wavelength 0.92 Å over a 360° wedge using 1° oscillations. We integrated and scaled reflections in HKL2000 (ref. 35) with separate scaling of anomalous pairs. We determined phases by single-wavelength anomalous dispersion (SAD) using Phaser HYSS[36]. We improved electron density maps by solvent flattening (RESOLVE)[37,38] in PHENIX AutoSol Wizard[36,39]. We manually modeled DNA and protein using Coot[40]. Automated refinement (Refmac5)[41] and manual modeling produced R_{work} and R_{free} values of 17.7% and 21.5%, respectively. We validated the structure using SFCHECK[42], PROCHECK[43] and Coot. In the final model, 100% of Ramachandran plot values fell into favored regions.

We made figures and alignments of DmTHAP with NMR structures using PyMOL[44]. We performed homology modeling of human THAP proteins using PHYRE[45]. We calculated DNA distortion using 3DNA (ref. 46) and CURVES+ (ref. 47). We made structure-based multiple sequence alignments with 3DCoffee[48,49] and JalView[50].

hTHAP9 SELEX. We performed SELEX experiments as described previously[51] and modified by N. Ogowa and M. Biggin (personal communication). Briefly, we incubated ~0.4 mg of recombinant hTHAP9 with 50 μl of TALON superflow (Clontech). We diluted saturated beads 1:5 with unbound resin and used ~10 μl of this slurry in binding experiments. We prepared random target dsDNA by PCR extension with the oligos 5′-GGATTTGCTGGTGCAGTAC AGTGGATCC-[N_{16}]-GGATCCCTTAGGAGCTTGAAATCGAGCAG-3′ and 5′-CTGCTCGATTTCAAGCTCCT-3′. We incubated 10 μl of protein slurry with random DNA (~1–2 ng), in a 20-μl reaction in 1× SELEX buffer (10 mM Tris-HCl, 7.6, 50 mM NaCl, 5% (v/v) glycerol, 0.1% (v/v) NP-40, 10 μM $ZnCl_2$, 5 mM $MgCl_2$), supplemented with 1 μg BSA (NEB) and 1 μg poly(dI-dC). The binding proceeded for 20 min at room temperature, then we washed twice with wash buffer (SELEX buffer with 5 mM NaCl), and eluted in 100 μl elution buffer (SELEX buffer with 500 mM NaCl). We PCR amplified this fragment using 20 cycles with the primers 5′-GGATTTGCTGGTGCAGTACA-3′ and 5′-CTGCTCGATTTCAAGCTCCT-3′. After four rounds of selection, >10% of the starting material was retained, amplified and subsequently sequenced using concatemerization[51]. We made sequence logos using the Delila program[52] with 76 independent sites.

35. Otwinowski, Z. & Minor, W. Processing of X-ray diffraction data collected in oscillation mode. in *Methods in Enzymology* Vol. 276 (eds. Carter, C.W.J. & Sweet, R.M.) 307–325 (Academic Press, Boston, 1997).
36. Zwart, P.H. *et al.* Automated structure solution with the PHENIX suite. *Methods Mol. Biol.* **426**, 419–435 (2008).
37. Terwilliger, T.C. Maximum-likelihood density modification. *Acta Crystallogr. D Biol. Crystallogr.* **56**, 965–972 (2000).
38. Terwilliger, T.C. Maximum-likelihood density modification using pattern recognition of structural motifs. *Acta Crystallogr. D Biol. Crystallogr.* **57**, 1755–1762 (2001).
39. Adams, P.D. *et al.* PHENIX: building new software for automated crystallographic structure determination. *Acta Crystallogr. D Biol. Crystallogr.* **58**, 1948–1954 (2002).
40. Emsley, P. & Cowtan, K. Coot: model-building tools for molecular graphics. *Acta Crystallogr. D Biol. Crystallogr.* **60**, 2126–2132 (2004).
41. Murshudov, G.N., Vagin, A.A. & Dodson, E.J. Refinement of macromolecular structures by the maximum-likelihood method. *Acta Crystallogr. D Biol. Crystallogr.* **53**, 240–255 (1997).
42. Vaguine, A.A., Richelle, J. & Wodak, S.J. SFCHECK: a unified set of procedures for evaluating the quality of macromolecular structure-factor data and their agreement with the atomic model. *Acta Crystallogr. D Biol. Crystallogr.* **55**, 191–205 (1999).
43. Laskowski, R.A., MacArthur, M.W., Moss, D.S. & Thornton, J.M. PROCHECK: A program to check the stereochemical quality of protein structures. *J. Appl. Crystallogr.* **26**, 283–291 (1993).
44. DeLano, W.L. *The PyMOL Molecular Graphics System* (DeLano Scientific, San Carlos, California, USA, 2002).
45. Kelley, L.A. & Sternberg, M.J. Protein structure prediction on the Web: a case study using the Phyre server. *Nat. Protoc.* **4**, 363–371 (2009).
46. Lu, X.J. & Olson, W.K. 3DNA: a versatile, integrated software system for the analysis, rebuilding and visualization of three-dimensional nucleic-acid structures. *Nat. Protoc.* **3**, 1213–1227 (2008).
47. Lavery, R., Moakher, M., Maddocks, J.H., Petkeviciute, D. & Zakrzewska, K. Conformational analysis of nucleic acids revisited: Curves+. *Nucleic Acids Res.* **37**, 5917–5929 (2009).
48. Poirot, O., Suhre, K., Abergel, C., O'Toole, E. & Notredame, C. 3DCoffee@igs: a web server for combining sequences and structures into a multiple sequence alignment. *Nucleic Acids Res.* **32**, W37–40 (2004).
49. O'Sullivan, O., Suhre, K., Abergel, C., Higgins, D.G. & Notredame, C. 3DCoffee: combining protein sequences and structures within multiple sequence alignments. *J. Mol. Biol.* **340**, 385–395 (2004).
50. Waterhouse, A.M., Procter, J.B., Martin, D.M., Clamp, M. & Barton, G.J. Jalview Version 2: a multiple sequence alignment editor and analysis workbench. *Bioinformatics* **25**, 1189–1191 (2009).
51. Roulet, E. *et al.* High-throughput SELEX SAGE method for quantitative modeling of transcription-factor binding sites. *Nat. Biotechnol.* **20**, 831–835 (2002).
52. Schneider, T.D., Stormo, G.D., Yarus, M.A. & Gold, L. Delila system tools. *Nucleic Acids Res.* **12**, 129–140 (1984).

doi:10.1038/nsmb.1742